PSFC/JA-09-44

Plasma structures observed in gas breakdown using a 1.5 MW, 110 GHz pulsed gyrotron

Hidaka, Y., Choi, E.M., Mastovsky, I., Shapiro, M.A.,
Sirigiri, J.R., Temkin, R.J., Edmiston,
G.F.*, Neuber, A.A.*, Oda, Y.**

2009

* Center for Pulsed Power and Power Electronics, Department of Electrical and Computer Engineering and
  Physics, Texas Tech University, Lubbock, Texas 79409, USA

** Naka Fusion Research Institute, Japan Atomic Energy Agency, Naka, Ibaraki 311-0196, Japan

Plasma Science and Fusion Center
Massachusetts Institute of Technology
Cambridge MA 02139 USA

Abstract:

Regular, two-dimensional plasma filamentary arrays have been observed in gas breakdown experiments using a pulsed 1.5 MW, 110 GHz gyrotron. The gyrotron Gaussian output beam is focused to an intensity of up to 4 MW/cm^2. The plasma filaments develop in an array with a spacing of about one quarter wavelength, elongated in the electric field direction. The array was imaged using photodiodes; a slow camera, which captures the entire breakdown event; and a fast camera with a six nanosecond window. These diagnostics demonstrate the sequential development of the array propagating back towards the source. Gases studied included air, nitrogen, SF$_6$, and helium at various pressures. A discrete plasma array structure is observed at high pressure while a diffuse plasma is observed at lower pressure. The propagation speed of the ionization front for air and nitrogen at atmospheric pressure for 3 MW/cm^2 was found to be on the order of 10 km/s.

I. INTRODUCTION

There are numerous studies reported on gas breakdown at microwave frequencies[1-3] and at optical frequencies.[4,5] However, gas breakdown research results in the frequency range between these two regimes, specifically between 100 and 800 GHz, have only recently been reported.[6,7] This is mainly because of the dearth of millimeter wave sources that can generate megawatts of power to achieve gas breakdown. Currently, a gyrotron is the only device that can deliver such high power in this frequency range.[8,9] Ongoing development of higher output power from gyrotrons will make gas breakdown issues in transporting the output beam even more important in future millimeter wave systems. This concern is manifested by the recent extension of numerical studies on gas breakdown into the millimeter wave regime.[10,11]

In this paper, we present the experimental results of gas breakdown induced by a pulsed 1.5 MW, 110 GHz gyrotron in several gases at a range of pressures. The temporal behavior of the breakdown process is also reported. The present results are an extension of our previous study,[6] in which we reported the first observation of a regular two-dimensional array of filaments in atmospheric air breakdown at 110 GHz. These filaments are qualitatively different from, and should not be confused with, the well-known filaments observed in laser breakdown. In our experiments, the filaments develop transverse to the propagation direction, along the direction of the electric field

3

polarization. In laser breakdown, filaments are instead observed along the beam propagation axis.[12]

The present results include detailed experimental studies of the time dependence of the formation of these filaments, showing that the filamentary array propagates in time back towards the high power microwave source. We also find that at low pressure, large scale plasmas are observed without filamentation.

II. EXPERIMENTAL SETUP

The top-view schematic of our breakdown experimental setup is shown in Fig. 1. The Gaussian beam generated from the 1.5 MW, 110 GHz gyrotron [see Ref. 8 for more detailed schematic and information on the gyrotron] comes out of the gyrotron window. Three mirrors are used to propagate the beam to the breakdown chamber. A TPX lens of 9.2 cm focal length focuses the beam down to a 4 to 5 mm waist radius at the center of the chamber. The maximum experimentally achieved power density at this location was 4 MW/cm^2 (or 5.6 MV/m in peak electric field strength). When gas breakdown occurs, the emitted plasma light is captured by the following diagnostics: (i) a Hamamatsu C5331-11 avalanche photodiode (APD) module for determining the onset of the breakdown, (ii) a Hamamatsu S5668 series 16-element silicon photodiode array (PDA) for determining the propagation speed of the ionization front of the breakdown, (iii) a slow, black

and white (B&W) charge-coupled device (CCD) camera to capture an open-shutter image of an entire plasma breakdown event, and (iv) a fast, intensified CCD (ICCD) camera made by Andor Technology, which can be gated to expose its sensor for as short as 6 ns, and thus, allows us to see only a snapshot of the breakdown plasma state at a certain stage. The sensor of the slow camera is triggered by a TTL pulse from a Stanford Research Systems DG535 delay generator well before the microwave pulse arrives at the focal region, and kept open for a few hundred milliseconds resulting in the capture of all of the light emitted during the breakdown. The fast camera sensor is triggered and also gated by a TTL gate pulse from another delay generator with various delay times and gate widths. This enables us to freely select different plasma evolution stages of our interest. The other diagnostics include broadband microwave video detectors, which monitor the microwave beam power before and after the breakdown region. Figure 2 shows sample traces of several of these diagnostics. From the avalanche photodiode signal and the camera gate pulse, we can determine which evolution stage is represented by the plasma image captured by the fast camera. For example, Fig. 2 indicates the fast camera image taken for this shot shows the plasma state approximately 1 µs after the breakdown start. Due to the response time of the avalanche photodiode module and the noise floor, the determined gate pulse timing is estimated to be accurate to a few tens of nanoseconds.

III. EXPERIMENTAL RESULTS

A. Observation of Breakdown Plasma Structures

1. Ambient Air

A typical atmospheric air plasma image captured by the slow camera in the E-plane is shown in Fig. 3, indicating the filamentary structure elongated along the electric field polarization. In this view, the microwave beam is propagating from left to right, and the electric field is oscillating up and down. The plasma images shown in Fig. 4 were obtained using the ambient air at the pressure of 710 Torr. The black and white images were captured by the slow camera. In all of these images, and all the other images to follow, the Gaussian beam is propagating from left to right, and the electric field is oscillating in and out of the paper. That is, the images were taken in the H-plane. The incident power density in the focal region for this set of experiments was estimated to be 3.5-4 MW/cm^2. The pseudo-color images in Fig. 4 were acquired by the fast gated camera with 49 ns optical gate width in each case. The gate pulse delay times from the start of breakdown were 400 ns, 1.28 µs and 1.52 µs, for Figs. 4(a), (b), and (c), respectively. The color images thus show the evolution in time of the breakdown in the gas, as opposed to the black and white images that show the breakdown integrated over the entire breakdown event. The three pairs of black and white images and color images were taken with different pulses (or shots) from the gyrotron. We draw the

following conclusions from these images:

First, as time passes, the plasma is moving to the left. Thus, we see explicitly that the breakdown plasma propagates toward the microwave source, as we reported in our previous measurements using two axially displaced photodiodes.[6] Secondly, the filaments existing at an earlier stage are extinguished at a later stage. The upstream filaments, which are being created closer to the microwave source with increasing time, absorb and reflect most of the incident power, resulting in the downstream filaments being extinguished. Therefore, the breakdown plasma does not expand, but rather propagates towards the source. Thirdly, and most importantly, the series of fast camera images have experimentally confirmed that the sequential development of the plasma filamentary array is indeed occurring as we hypothesized in our purely electromagnetic wave model described in Ref. 6. That model predicts that after the formation of a first filament, subsequent filaments will be created upstream of that filament, with a spacing of about a quarter-wavelength.

Figure 5 shows the plasma images of ambient air at 440 Torr, with the fast camera optical gate width of 49 ns. The observed plasma structure is no longer a simple array of filaments. The beam waist is located roughly at the center of these images in this case. Near the focal region, the plasma appears diffuse with some discrete spots. The plasma tends to be discrete on either side of the focal region. The upstream plasma is different from the downstream plasma in that the array is radially more expanded in the upstream region. Also note that the size of the breakdown region is

7

much larger compared to the atmospheric pressure case shown in Fig. 4. This is mainly because the

breakdown threshold is lower at this lower pressure. Thus, the initial breakdown event occurs in the

early stage of the microwave pulse. Then, the breakdown plasma has a much longer time to

propagate towards the source. In addition, as shown later, the speed of the ionization front

propagates faster at lower pressures. These two effects explain the much larger plasma images

captured by the slow camera.

2.   Nitrogen

Breakdown phenomena in other gases are of great interest since the breakdown depends on

plasma chemistry, which differs from gas to gas. Figure 6 shows the breakdown images of nitrogen

plasma at 780 Torr, with the optical gate width of 6 ns for the fast camera images. The estimated

power density in the focal region for this set of experiments was 3-3.5 MW/cm^2. Both the slow and

fast camera images resemble those of the ambient air plasma at atmospheric pressure as shown in

Fig. 4. Hence, it is determined that the presence of oxygen in air has no critical role in generating the

observed regular filamentary array. All the observations made regarding air breakdown as seen in

Fig. 4 apply to the nitrogen plasmas at atmospheric pressure in Fig. 6.

The plasma images for nitrogen at 360 Torr and 2 Torr are shown in Fig. 7, with the optical

gate being 6 ns long for the fast camera. Again, the plasma images of nitrogen are similar to those of

air as shown in Fig. 5. The interesting feature observable in the slow camera images of Figs. 7(a)-(b)

is a transition from a diffuse plasma to a sheet-like plasma, and then to a discrete filamentary plasma.

In Fig. 7(a), there exists a diffuse plasma to the right of the intense plasma shown by the fast camera image. Slightly to the left of this diffuse plasma, plasma sheets, represented by thin curved lines, can be observed. Finally, further to the left, a discrete filamentary plasma array appears, although the isolation between the filaments in the transverse direction is not as good as in the atmospheric pressure case. Note that the typical distance between the sheets is approximately a quarter-wavelength of the 110 GHz microwave beam. This is the same distance as was predicted by our previous diffraction model to explain the formation of the regular array in atmospheric air breakdown. Also note the remarkably high reproducibility (in terms of size and shape) of the breakdown images from the slow camera for three different shots at this pressure.

Below 2 Torr, nitrogen breakdown could not be achieved with the available power and pulse length. Figure 7(d) shows a typical nitrogen plasma image observed at 2 Torr. No filamentary or discrete structure is observed. The fact that the fast camera image also shows no sign of filamentation excludes the possibility of the plasma evolution scenario in which a filamentary plasma exists at a certain stage, but is smeared out by diffusion later. This result clearly indicates that high gas pressure is essential for the observed filamentation.

3. SF_6

Figure 8 shows the SF_6 plasma image at 195 Torr with the power density of ~3 MW/cm^2 in

the focal region. No breakdown could be achieved above 300 Torr. The slow camera images show a large diffuse plasma, partly because the sensor was oversaturated. However, the fast camera images show that the plasma structure does still have some discreteness, even though the filaments in the SF_6 plasma are not well isolated compared with those in air and nitrogen plasmas at high pressure. In Fig. 9, breakdown images of SF_6 at 115 Torr are shown. Each filament appears to have even less separation in the upstream region than in Fig. 8 in the fast camera images. Compared to air and nitrogen, the array-like regular structure no longer exists. Tiny spots (filaments) are all randomly distributed.

4.   Helium

Figure 10 shows helium breakdown plasma images at 730 Torr, which reveal a plasma evolution vastly different from that of air and nitrogen. The power density was 2.5 – 3 MW/cm^2 in the focal region. The downstream (right) side shows discrete plasmas, but qualitatively different from the array structure observed in air and nitrogen at atmospheric pressure. On the other hand, the upstream (left) side shows diffuse plasmas. Furthermore, the most significant difference from all the previous gas species, at all the pressures investigated, is that there exists a secondary plasma evolution after the first one. In Figs. 10(a) and (b), there is no light emission on the downstream side in the fast camera images, and the plasma appears to propagate upstream. In Fig. 10(c), the first plasma moved out of the camera view, but a second plasma suddenly appears in the downstream

region. This second plasma then propagates towards the source as shown in Fig. 10(d).

The presence of the second plasma evolution was also observed at a much lower pressure of 1.2 Torr as shown in Fig. 11, with the power density of $3 - 3.5$ MW/cm^2. At every stage, the plasma is very diffuse. The initial plasma, as seen by the fast camera, quickly propagates upstream as shown in Fig. 11(b). However, in Fig. 11(c), the plasma light emission is completely extinguished out of the camera view, then the emission comes back as shown in Fig. 11(d). Figure 12 shows the traces of the incident power, avalanche photodiode and camera gate pulse for the shot shown in Fig. 11(c). The gate pulse is exactly at the dip of the avalanche photodiode signal. The fact that the avalanche photodiode signal rises again after the microwave pulse is turned off indicates that the second plasma evolution, or, rather, emission, is not coming from a newly generated plasma, but from the old existing plasma as a delayed emission.

As evident from these results, plasmas generated by the 110 GHz microwave beam in different gas species and at different pressures manifest qualitatively different structures as well as evolution patterns.

B. Ionization Front Propagation Speed

The propagation speed of the ionization front has been estimated from the available fast camera images. The ionization front position is plotted against the camera gate pulse delay time, so that the propagation speed can be estimated from its slope. Such a plot for air and nitrogen at

11

atmospheric pressure with the incident power density of about 3 MW/cm^2 is shown in Fig. 13. The

estimated speed was 14 km/s for air and 12 km/s for nitrogen. Note that the fitted line for air does

not go through the zero position. This is due to the fact that the incident power level for the air

breakdown data was slightly higher than that for the nitrogen breakdown data. To estimate the speed

with a roughly equal power density, a line fit region for air was selected farther away from the beam

waist, resulting in the vertical shift of the fitted line for air with respect to the fitted line for nitrogen.

Figure 14 shows the pressure dependence of the propagation speed for the incident power

density of roughly 1.5–2 MW/cm^2. Note that, in Fig. 14, there are two sets of estimation. One is

labeled as "ICCD", which is estimated from the fast camera images. The other, "PDA" is estimated

from the photodiode array signals. They both agree reasonably well. The effect of microwave power

intensity may seem rather large, comparing the propagation speed of 14 km/s for a microwave beam

intensity of 3 MW/cm^2 and 5 km/s for 1.5-2 MW/cm^2 in the case of atmospheric air breakdown.

However, the ionization rate of air scales approximately as the electric field strength to the fifth

power.[13] This implies a roughly 3 to 6 times faster ionization rate for the higher intensity case than

for the lower intensity case. Hence, the substantial increase in the estimated propagation speed

appears reasonable. As for pressure dependence, the speed increases from 5 km/s at atmospheric

pressure to 20 km/s at 420 Torr. This makes sense because the breakdown threshold decreases as the

pressure decreases so that ionization occurs much more rapidly, and so does the propagation of the

ionization front. The propagation speed estimated at pressures lower than 400 Torr has been omitted due to a measurement reliability issue. First, the light emission intensity is lowered so that a worse signal-to-noise ratio makes the determination of the onset of light emission difficult. Secondly, the speed is estimated from the slope of the position vs. time. As the speed becomes large, the error associated with the slope becomes too large.

IV. DISCUSSION AND CONCLUSIONS

The snapshots at different stages of the breakdown plasma have directly verified that the formation of the regular filamentary plasma array in atmospheric air proceeds sequentially from the initial breakdown region upstream, towards the high power microwave source. This result agrees with our model based on microwave beam diffraction presented in Ref. 6.

Taking both open-shutter images and fast gated images of the breakdown plasma in different gases at different pressures, we observed vastly different plasma evolution behavior. In general, high pressures resulted in more discrete plasma structures, whereas low pressures produced diffuse plasmas. The ionization front propagation speed was estimated to be on the order of 10 km/s in air and nitrogen at atmospheric pressure for ~3 MW/cm^2, and increased as the pressure of air and nitrogen was decreased.

The present study indicates that breakdown filaments induced by high frequency microwaves, which occur transverse to the beam propagation direction, differ substantially from laser breakdown in which filaments appear along the propagation direction. Discrete plasma structures have been reported at lower microwave frequencies in the past[14-17] with some attempts to theoretically explain the emergence of such structures.[18-21] Some of these results are similar to the 110 GHz breakdown plasmas reported here, in terms of the direction of filamentation. Yet, the clarity and regularity of the plasma filamentary array generated by the 110 GHz microwaves reported here are unprecedented and are not adequately explained by these theories.

Further research and analysis will be needed to explain many of the details of the research reported here. At present, we do not have a conclusive explanation for the development of an initial, intense filament at the breakdown region. The physical model of the filament growth from an initial tiny spherical plasmoid due to the field enhancement in the poles and the field reduction in the equator described in Ref. 21 may be applicable to the filamentation observed in the 110 GHz microwave breakdown. So far, however, there has been no direct experimental evidence to support this model. Our theory instead is aimed at explaining the development of a subsequent filamentary array, as a result of diffraction and reflection from the initial filament. We also do not have an explanation of the transition from a filamentary array breakdown to a more diffuse breakdown. A detailed theory of microwave breakdown and subsequent plasma evolution is needed to fully

understand these phenomena. Such a theory is beyond the scope of the present research effort, but a

promising theoretical advancement is already being made elsewhere,[22] and these fundamental

questions raised by the experimental results reported here might be answered more quantitatively in

the near future.

REFERENCES

[1] A. D. MacDonald, *Microwave Breakdown in Gases* (Wiley, New York, 1966).

[2] Y. P. Raizer, *Gas Discharge Physics* (Springer, Berlin, 1991).

[3] A. V. Gurevich, N. D. Borisov, and G. M. Milikh, *Physics of Microwave Discharges* (Gordon and Breach, Amsterdam, 1997).

[4] N. Kroll and K. M. Watson, Phys. Rev. A **5**, 1883 (1972).

[5] Y. P. Raizer, *Laser-Induced Discharge Phenomena* (Consultants Bureau, New York, 1977).

[6] Y. Hidaka, E. M. Choi, I. Mastovsky, M. A. Shapiro, J. R. Sirigiri, and R. J. Temkin, Phys. Rev. Lett. **100**, 035003 (2008).

[7] Y. Oda, K. Komurasaki, K. Takahashi, A. Kasugai, and K. Sakamoto, J. Appl. Phys. **100**, 113307 (2006).

[8] E. M. Choi, A. J. Cerfon, I. Mastovsky, M. A. Shapiro, J. R. Sirigiri, and R. J. Temkin, Fusion Sci. Technol. **52**, 334 (2007).

[9] K. Sakamoto, A. Kasugai, K. Takahashi, R. Minami, N. Kobayashi, and K. Kajiwara, Nature Physics, **3**, 411 (2007).

[10] S. K. Nam and J. P. Verboncoeur, Appl. Phys. Lett. **93**, 151504 (2008).

[11] A. A. Neuber, J. T. Krile, G. F. Edmiston, and H. G. Krompholz, Phys. Plasmas **14**, 057102 (2007).

[12] W. L. Kruer, *The Physics of Laser Plasma Interactions* (Westview Press, Boulder, 2001).

[13] W. C. Taylor, W. E. Scharfman, and T. Morita, *Advances in Microwaves*, edited by L. Young, (Academic, New York, 1971), Vol. 7.

[14] A. L. Vikharev, V. B. Gil'denburg, S. V. Golubev, B. G. Eremin, O. A. Ivanov, A. G. Litvak, A. N. Stepanov, and A. D. Yunakovskii, Sov. Phys. JETP **67**, 724 (1988).

[15] A. L. Vikharev, A. M. Gorbachev, A. V. Kim, and A. L. Kolysko, Sov. J. Plasma Phys. **18**, 554 (1992).

[16] V. G. Brovkin and Yu. F. Kolsenichenko, J. Mosc. Phys. Soc. **5**, 23 (1995).

[17] V. L. Bychkov, L. P. Grachev, and I. I. Isakov, Tech. Phys. **52**, 289 (2007).

[18] V. B. Gil'denburg and A. V. Kim, Sov. J. Plasma Phys. **6**, 496 (1980).

[19] O. A. Sinkevich and V. E. Sosnin, High Temp. **39**, 180 (2001).

[20] P. V. Vedenin and N. A. Popov, JETP **96**, 40 (2003).

[21] V. B. Gil'denburg, I. S. Gushchin, S. A. Dvinin, and A. V. Kim, Sov. Phys. JETP **70**, 645 (1990).

[22] S. K. Nam and J. P. Verboncoeur, "Theory of Filamentary Plasma Array Formation in Microwave Breakdown at Near Atmospheric Pressure," IEEE 36th International Conference on Plasma Science, San Diego, CA, May 31 – June 5, 2009 (IEEE Press, Piscataway, NJ, to be published).

Figure Captions:

Fig. 1: (Color online) Schematic of breakdown experiment.

Fig. 2: (Color online) Sample traces of avalanche photodiode (APD), fast camera gate pulse, microwave diode signals for incident and transmitted power, for a pulse with a gas breakdown event. Note that the units differ for each trace.

Fig. 3: Typical image captured by the slow camera in ambient air breakdown, viewing in the plane containing E and k (the E-plane). Note the development of the filaments along the direction of the E field.

Fig. 4: (Color online) Images of breakdown in ambient air at 710 Torr with 49 ns optical gate pulse starting at (a) t = 400 ns, (b) 1.28 µs, and (c) 1.52 µs. The image is taken in the plane containing H and k, the H-plane.

Fig. 5: (Color online) Ambient air at 440 Torr with 49 ns optical gate starting at (a) t = -40 ns, (b) 480 ns, and (c) 720 ns.

Fig. 6: (Color online) Nitrogen at 780 Torr with 6 ns optical gate pulse starting at (a) t = 360 ns, (b) 710 ns, and (c) 1.25 µs.

Fig. 7: (Color online) Nitrogen at 360 Torr with 6 ns optical gate pulse starting at (a) t = 170 ns, (b) 620 ns, and (c) 1.41 µs, and at 2 Torr with 6 ns-long optical gate pulse starting at (d) 100 ns. The scale shown in (c) applies to (a)-(c).

Fig. 8: (Color online) SF6 at 195 Torr with 6 ns optical gate pulse starting at (a) t = 110 ns and (b) 1.34 µs.

Fig. 9: (Color online) SF6 at 115 Torr with 6 ns optical gate pulse starting at (a) t = 220 ns and (b) 1.45 µs.

Fig. 10: (Color online) Helium at 730 Torr with 6 ns optical gate pulse starting at (a) t = 40 ns, (b) 130 ns, (c) 650 ns, and (d) 2.48 µs.

Fig. 11: (Color online) Helium at 1.2 Torr with 6 ns optical gate pulse starting at (a) t = 40 ns, (b) 160 ns, (c) 1.14 µs, and (d) 1.92 µs.

Fig. 12: (Color online) Oscilloscope traces of APD, camera gate pulse, microwave diodes for incident and transmitted power for the shot shown in Fig. 10(c).

Fig. 13: (Color online) Ionization front position vs. gate pulse delay in air and nitrogen at atmospheric pressure for incident power intensity of ~3 MW/cm^2. The dotted lines show the fit for the propagation speed of the ionization front.

Fig. 14: (Color online) Ionization front propagation speed vs. pressure for a microwave beam intensity of 1.5-2 MW/cm^2. "PDA" and "ICCD" values are estimated from the photodiode array signals, and from the fast camera images, respectively.
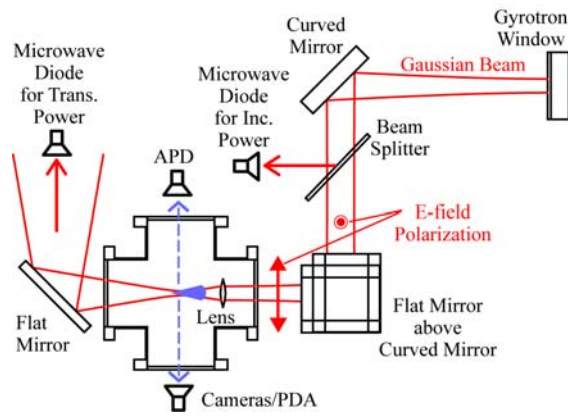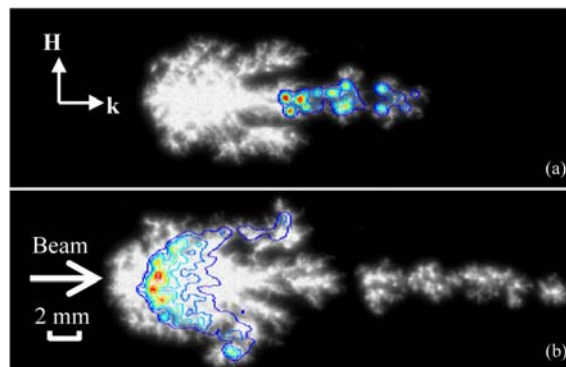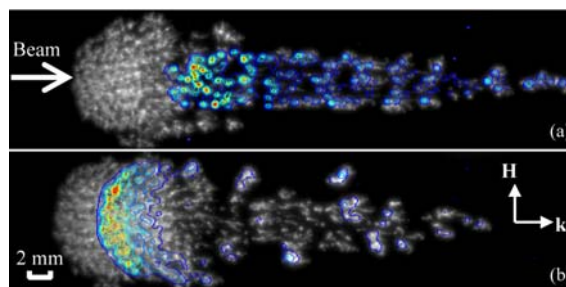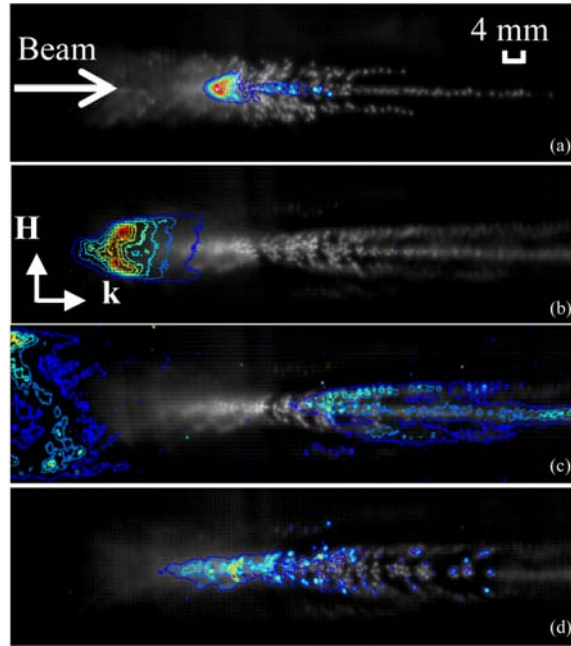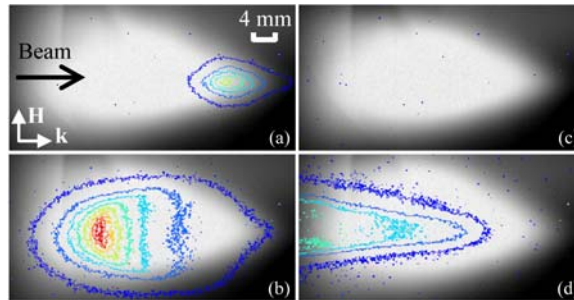
Fig. 1
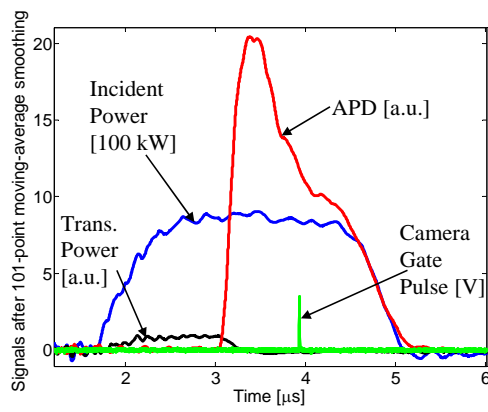
Fig. 2
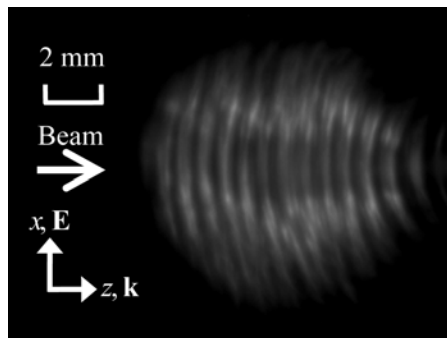
Fig. 3
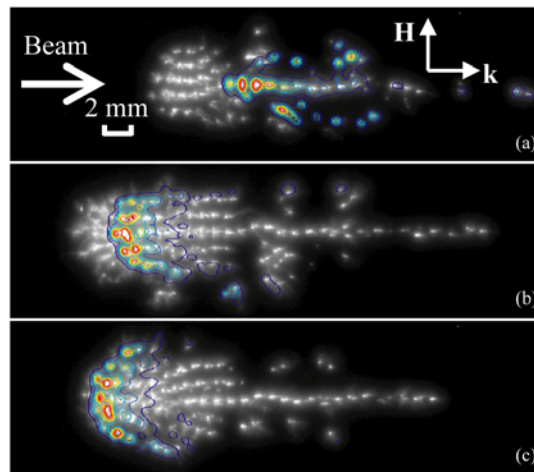
Fig. 4
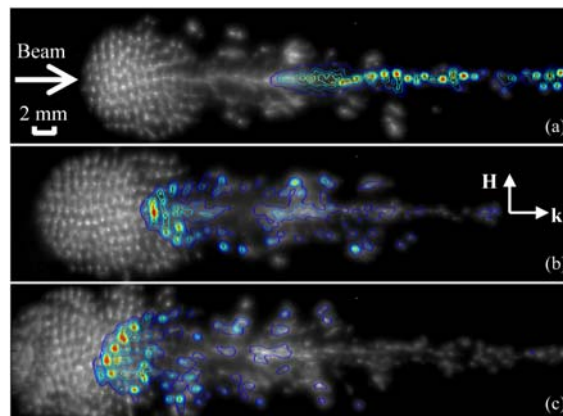
Fig. 5
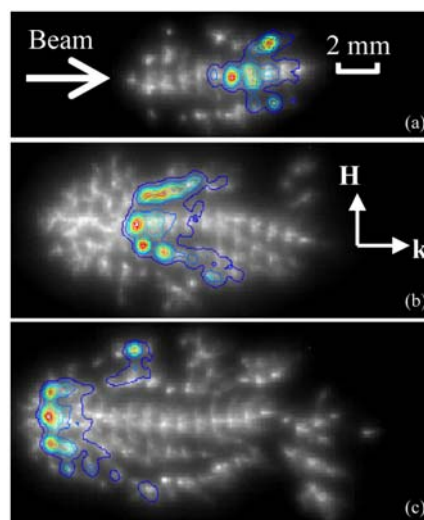
Fig. 6
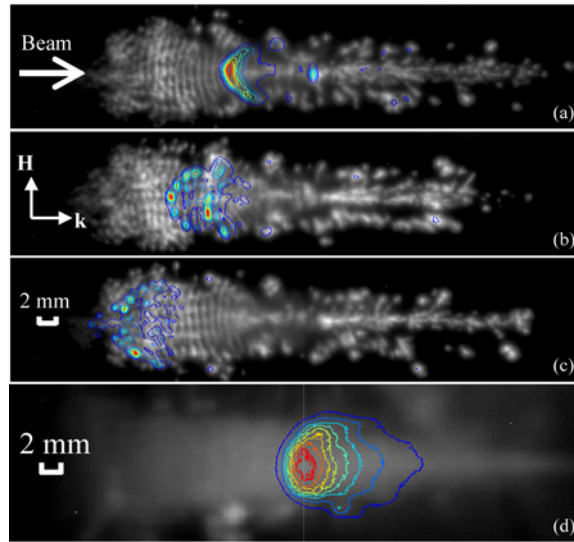
Fig. 7

Fig. 8

Fig. 9

Fig. 10

Fig. 11

Fig. 12

Fig. 13

Fig. 14